SEISMIC MODEL OF THE GAS COOLED FAST BREEDER REACTOR CORE SUPPORT STRUCTURE*

L.E. PENZES, K.H. CHANG, G.E. LEE
General Atomic Company, San Diego, California 92138, U.S.A.

SUMMARY

The modeling technique for the seismic analysis of the core support structure of a gas cooled fast breeder reactor is developed.

The core support structure consists of the support cylinder and a perforated grid plate from which 265 fuel and blanket elements are suspended as cantilevered beams. Due to limitations of computer storage and considering the large number of core elements, well planned seismic modeling technique is very important to obtain a realistic analysis. The analysis of the core support structure consists of three steps: (a) analysis of the grid plate, (b) analysis of the core elements, and (c) modal synthesis.

The dynamic theory of the grid plate is developed by generalizing Reissner-Mindlin thick plate theory with orthotropic constants and then modify the formulations of the rotary inertia expressions to include the rotary inertia effects of the core elements.

In this general case the differential equation for this problem can be solved by numerical techniques. However, applying the effective elastic constants of the perforated plate in the customary fashion the solution can be determined analytically in terms of Bessel functions.

By applying the present technique, it is shown that the grid plate fundamental frequency is in the range of the fundamental frequencies of the core elements so that a dynamic coupling effect exists.

Due to this dynamic coupling effect the grid plate cannot be considered a "rigid plate" for the purposes of seismic analysis of the gas cooled fast breeder reactor. Hence, a simple spring-mass seismic model is inadequate and a more elaborate finite element seismic model applying plate and shell elements is used instead.

The technique of modal synthesis is then applied to determine the effects of dynamic coupling and to study the seismically induced motions of the core elements in a realistic manner.

* Work supported by the U.S. Atomic Energy Commission under Contract AT(04-3)-167, Project Agreement 23.

1. Introduction

A new modeling technique for the seismic analysis of the GCFR core support structure is under development. In previous analyses a single-beam, lumped-mass model was used as a first approximation. With the new technique one can determine what effect a large number of core elements, hanging as cantilevered beams from a perforated grid plate, have on the grid plate vibration. With this technique, the amplitudes and stresses of individual core elements can be computed. This method also permits the study, in a realistic manner, of the relative motions between the individual core elements.

The core support structure consists of the support cylinder and a perforated grid plate from which the 265 fuel and blanket elements are suspended as cantilevered beams. Because of the limitations of computer storage and running time, some simplifying assumptions are made to economize on the problem and yet still obtain a realistic analysis. For this reason, the analysis of the core support structure is divided into three steps:

1. Analysis of the grid plate,
2. Analysis of the core elements, and
3. Modal synthesis.

The major part of this paper addresses the dynamic behavior of the grid plate and its influence on the seismic analysis. The analysis of the fuel and blanket elements and the method of modal synthesis are also discussed. However, this latter method is still in the development stage and only a brief description is given.

2. Theory and Analysis of Grid Plate

Dynamic coupling exists between the grid plate and the core elements (fuel and blanket) if their vibrational frequency is in the same range. In this case the effect of the grid plate must be included in the seismic analysis of the core. Since this condition exists in the GCFR core, the computational method of the grid plate vibration is reviewed. To model a thick perforated plate with 265 fuel and blanket elements, attached to the plate as cantilevers, is a formidable and time-consuming task. For this reason, some simplifying assumptions are made.

The first assumption is that the fuel and blanket elements are attached to the grid plate as "rigid rods." In this case, the influence of the rigid rods can be represented by the mass and rotary inertia of each rod.

This method is based on the theories of Reissner and Mindlin [1,2], which are modified and supplemented according to GCFR needs. The isotropic thick plate theory of Reference [2], modified with orthotropic constants, is used for the investigation. By including the effect of rigid rods, with their masses and rotary inertias, in the analysis of the grid plate, the problem is reduced to the vibration problem of an orthotropic thick plate. This solution is valid for general homogeneous boundary conditions of the thick plate. For a further improvement in the physical model of the grid plate analysis, the perforated plate is connected to an elastic ring at the periphery of the plate and the effect of this ring on the vibration of the perforated plate is investigated. To the authors' knowledge, this type of application of thick plate theory is new in the technical literature.

2.1 Mathematical Formulation

The stress-strain relations of plate theory are expressed according to eq. (5.4.8) of Reference [3], assuming symmetry with respect to a plane, as

$$\left.\begin{aligned} \sigma^{ij} &= C^{ij}_{rs}\varepsilon^{rs} \\ \sigma^{33} &= 0 \end{aligned}\right\} \qquad i,j,r,s = 1,2,3 \tag{1}$$

and

$$C^{ij}_{3s} = C^{3s}_{ij} = C^{33}_{i3} = C^{i3}_{33} = 0 \qquad i,j,s = 1,2$$

where σ^{ij} = stress tensor,
C^{ij}_{rs} = anisotropic plate coefficient,
ε^{rs} = strain tensor.

The displacement relations are

$$u_i = Z\psi_i, \qquad u_3 = W \tag{2}$$

where $i = 1,2$,
ψ_i = rotation components,
W = transverse displacement,
Z = normal coordinate of the plate.

The bending and twisting moments can be expressed as

$$M_{ij} = \int_{-h/2}^{h/2} \sigma_{ij} Z \, dZ \tag{3}$$

where $i, j = 1, 2$,
h = thickness of the plate.

The shear forces of the plate are defined as

$$Q_i = \int_{-h/2}^{h/2} \sigma_{i3} \, dZ \tag{4}$$

where $i = 1,2$.

The strain displacements relations, in terms of physical components, are

$$\varepsilon_{(ii)} = \left(\frac{u_{(i)}}{\sqrt{g_{(ii)}}}\right)_{,(i)} + \frac{1}{2g_{(ii)}} \left(g_{(ii)}\right)_{,k} \frac{u_k}{\sqrt{g_{kk}}} \tag{5}$$

$$\varepsilon_{(ij)} = \frac{1}{2\sqrt{g_{(ii)}g_{(jj)}}} \left[g_{(ii)} \left(\frac{u_{(i)}}{\sqrt{g_{(ii)}}}\right)_{,(j)} + g_{(jj)} \left(\frac{u_{(i)}}{\sqrt{g_{(jj)}}}\right)_{,(i)} \right] \qquad i \neq j \tag{6}$$

where the indices in parentheses are not summed and $g_{11} = g_{33} = 1$, $g_{22} = r^2$. The strain displacement eqs. (5) and (6) are expressed in terms of rotation (ψ_1) and transverse

displacement (W), shown in eq. (2). The strain relations as expressed by eqs. (5) and (6), with the substitution for the ψ_1 and W included, are then inserted into the stress-strain relations of eq. (1). The next step is the substitution of the stress-strain relations, in eq. (1), into eqs. (3) and (4), thus obtaining the moment and shear forces in terms of ψ_1 and W. Finally, the differential equations for the thick anisotropic plate are derived by substituting the modified eqs. (3) and (4) into the equilibrium eq. (2) of Reference [2].

$$D_{11}\frac{\partial^2\psi_r}{\partial r^2}+\frac{D_{12}}{r}\frac{\partial\psi_r}{r}-\left(D_{13}+\frac{D_{14}}{r^2}\right)\psi_r+\frac{D_{15}}{r^2}\frac{\partial^2\psi_r}{\partial\theta^2}+\frac{D_{16}}{r}\frac{\partial^2\psi_\theta}{\partial r\partial\theta}-\frac{D_{17}}{r^2}\frac{\partial\psi_\theta}{\partial\theta}-D_{18}\frac{\partial W}{\partial r}=I_r\frac{\partial^2\psi_r}{\partial t^2} \tag{7}$$

$$\frac{D_{21}}{r}\frac{\partial^2\psi_r}{\partial r\partial\theta}+\frac{D_{22}}{r^2}\frac{\partial\theta_r}{\partial\theta}+\frac{D_{23}}{r}\frac{\partial^2\psi_r}{\partial r\partial\theta}+D_{24}\frac{\partial^2\psi_\theta}{\partial r^2}+\frac{D_{25}}{r}\frac{\partial\psi_\theta}{\partial r}$$

$$-\left(D_{26}+\frac{D_{27}}{r^2}\right)\psi_\theta+\frac{D_{28}}{r^2}\frac{\partial^2\psi_\theta}{\partial\theta^2}-\frac{D_{29}}{r}\frac{\partial W}{\partial\theta}=I_\theta\frac{\partial^2\psi_\theta}{\partial t^2} \tag{8}$$

$$D_{31}\left(\frac{\partial\psi_r}{\partial r}+\frac{\psi_r}{r}\right)+\frac{D_{32}}{r}\frac{\partial\psi_\theta}{\partial\theta}+D_{33}\left(\frac{\partial^2W}{\partial r^2}+\frac{1}{r}\frac{\partial W}{\partial r}\right)+\frac{D_{34}}{r^2}\frac{\partial^2W}{\partial\theta^2}=\rho h_m\frac{\partial^2W}{\partial t^2} \tag{9}$$

where D_{ij} = orthotropic constants,
I_r, I_θ = arbitrary rotary inertia in the radial and tangential directions,
h_m = effective plate thickness,
ρ = density of plate.

The solution is obtained similar to that of Mindlin [2]:

$$\psi_r=k_1\frac{\partial W_1}{\partial r}+k_2\frac{\partial W_2}{\partial r}+\frac{k_3}{r}\frac{\partial H}{\partial\theta} \tag{10}$$

$$\psi_\theta=\frac{k_4}{r}\frac{\partial W_1}{\partial\theta}+\frac{k_5}{r}\frac{\partial W_2}{\partial\theta}+k_6\frac{\partial H}{\partial r} \tag{11}$$

$$W=W_1+W_2 \tag{12}$$

where $k_1, \cdots, k_6$ are functions of the elastic constants and the unknown frequency. By substituting eqs. (10), (11), and (12) into eqs. (7), (8), and (9), the resulting equations can be solved by some numerical techniques such as the finite-difference and predictor-corrector methods.

Application of the equivalent solid-plate theory to the perforated plates reduces the elastic constants to an effective modulus of elasticity and Poisson's ratio.

A similar mathematical treatment can be used for the isotropic case solved by Mindlin [2], and the resulting differential equations are reduced to

$$(\nabla^2+\Omega_1^2)\,W_1=0 \tag{13}$$

$$(\nabla^2+\Omega_2^2)\,W_2=0 \tag{14}$$

$$(\nabla^2 + \Omega_3^2)\, H = 0 \tag{15}$$

where

$$\nabla^2 = \left(\frac{\partial^2}{\partial r^2} + \frac{1}{r}\frac{\partial}{\partial r} + \frac{1}{r^2}\frac{\partial^2}{\partial \theta^2}\right) \tag{16}$$

$$\left.\begin{aligned} \Omega_1^2 &= \frac{k_1 I_p^2 - D_{18}(1 + k_1)}{D\, k_1} \\ \Omega_2^2 &= \frac{k_2 I_p^2 - D_{18}(1 + k_2)}{D\, k_2} \\ \Omega_3^2 &= \frac{2(I_p^2 - D_{18})}{D(1 - \tilde{\nu})} \end{aligned}\right\} \tag{17}$$

$$D = \frac{\tilde{E}}{(1 - \tilde{\nu}^2)}\frac{h^3}{12} \qquad D_{18} = k^2 \tilde{G} h \qquad k^2 = \frac{\pi^2}{12} \tag{18}$$

$\tilde{E}$ = effective modulus of elasticity,

$\tilde{G}$ = effective modulus of shear,

$\tilde{\nu}$ = effective Poisson's ratio.

The solution of eqs. (13), (14), and (15) are obtained as

$$W = W_1 + W_2 = A\, J_m(\Omega_1 r) + B\, J_m(\Omega_2 r) \tag{19}$$

$$H = C\, J_m(\Omega_3 r)$$

and depend on the arguments of the coefficients Ω_1, Ω_2, and Ω_3.

Any homogeneous boundary conditions can now be applied at the edge of the plate.

The concept of a grid plate, which is a perforated plate with an attached ring, is illustrated in Figure 1. The ring is simply supported and the following boundary conditions are considered for the combined system; superscript (r) designates the ring.

$$W^{(r)}\Big|_{r=b} = 0 \qquad M_r^{(r)}\Big|_{r=b} = 0 \qquad W^{(r)}\Big|_{r=a} = W\Big|_{r=a}$$

$$\psi_r^{(r)}\Big|_{r=a} = \psi_r\Big|_{r=a} \qquad M_r^{(r)}\Big|_{r=a} = M_r\Big|_{r=a} \qquad Q_r^{(r)}\Big|_{r=a} = Q_r\Big|_{r=a} \tag{20}$$

With substitution of eqs. (17) and (19) into boundary condition (20), the unknown constants and the frequency p can be determined.

In reviewing and verifying the different effects of the present theory, an interesting point is that the elimination of the transverse shear effect reduces the differential eqs.(7), (8), and (9) to the following simple expression:

$$(L + \lambda_1^2)(L - \lambda_2^2)\, W = 0 \tag{21}$$

where

$$L = \frac{\partial^2}{\partial r^2} + \frac{1}{r}\frac{\partial}{\partial r} + \frac{1}{r^2}\frac{\partial^2}{\partial \theta^2}$$

$$\lambda_{1,2}^2 = \pm \mu^2 + (\mu^4 + \lambda^4)^{1/2} \tag{22}$$

$$\lambda^4 = \frac{\delta h}{D} p^2 \qquad \mu^2 = \frac{Ip^2}{2D} \tag{23}$$

Eliminating the rotary inertia I = 0 reduces eq. (21) to the well-known equation of a vibrating plate (eq. 94.1, Reference [5]).

2.2. Numerical Examples

For the numerical determination of the grid-plate frequencies, the following constants are considered:

a = 53.5 in.	h = 24 in.	$\rho_{plate} = 4.8 \times 10^{-4}$ lb-sec^2/in.^{4}
b = 60 in.	I = 432 lb-sec^2/in.	$\rho_{core} = 3.7 \times 10^{-3}$ lb-sec^2/in.^{4}
$\tilde{E} = 5.08 \times 10^5$ psi	$\tilde{\nu} = 0.762$	$\rho_{ring} = 7.5 \times 10^{-4}$ lb-sec^2/in.^{4}
$E_{ring} = 2.54 \times 10^7$ psi	$\nu_{ring} = 0.3$	

The different effects on the plate vibration were reviewed, and the computed frequencies are shown in Figure 2. For Case 1, the plate is considered fixed at radius a, without the ring. The frequency was computed using the customary formula for a thin plate [4].

For the following cases, the computation of the vibrating mass includes both the mass of the plate and the mass of the core. For Case 2, the effect of rotary inertia and for Case 3, the terms of transverse shear were added to the computation. Finally, for Case 4, the simply supported ring was added to the perforated plate.

2.3. Conclusions

It is evident from Figure 2 that the rotary inertia and transverse shear have very significant effects when computing the natural frequency of the grid plate. Consequently, these effects will also be included in the seismic response of the GCFR core support structure.

3. Analysis of Core Elements

There are three types of GCFR core elements: fuel elements, control-rod fuel elements, and radial blanket elements. Fuel elements contain 270 fuel rods and one thermocouple rod, each 7.16 mm (0.282 in.) in diameter. Blanket elements contain 126 blanket rods and one thermocouple rod, each 12.8 mm (0.504 in.) in diameter. The rods in the elements are cantilevered from their top end and are arranged in a hexagonal lattice pattern. The rods are supported at nine axial locations by spacer grids. The spacer grids are designed to maintain the lattice structure but still allow axial movement to accommodate differential motion between the rods and the element duct. The rods are not otherwise restrained.

The overall length of a fuel element is about 11.5 ft and its gross weight is about

620 lb. A blanket element is similar to a fuel element, but its gross weight is higher—about 910 lb.

There are 265 elements in the reactor core. The elements are secured by locking the top cylindrical portion of each element into a corresponding hole in the supporting grid plate. This arrangement forms a very secure joint. A schematic of the locking mechanism is presented in Figure 3.

Two representations of a grid plate to core element joint are considered. In the first, the element is clamped to the lower edge of the plate (see Figure 4). This is valid for moderate excitations. For larger excitations, the mating surfaces at the lower edge of the grid plate may separate. In this case a pinned-pinned representation is considered (see Figure 5).

To analyze these two cases, a finite-element model of the core element was developed for use with the SAP IV computer program. The model consisted of 30 beam elements and 32 modal points. Seventeen beams were used to model the rod bundle; the remaining thirteen beams were used for the element duct. It was assumed that the spacer grids acted as rigid links between the element duct and the rod bundle. It was further assumed that the spacer grids act as simple supports for the rod bundle.

Because of large temperature variations from one end of the element to the other, a significant change of elastic properties occurs along the length. This effect was accounted for in the modeling.

With this model, modal extractions were performed for the two cases described above. The calculated fundamental frequency of fuel element bending was 11.2 Hz for the clamped-end condition and 9.3 Hz for the pinned-end condition. The corresponding frequencies for the blanket elements were 9.4 Hz and 7.7 Hz, respectively.

4. Modal Synthesis

Because the frequencies of the core elements are in the same range as the grid plate, the coupling effect between the two systems must be determined. There are several methods to determine this effect, one is by Hurty [6] and another by Gladwell [7].

A third method is the use of effective modal rotary inertias in the analysis of the grid plate. With this method the results of the previous two analyses can be superimposed in a more direct manner.

All these effects influencing the seismic analysis will be implemented in future work using the SAP IV code.

5. Conclusions

For the seismic analysis of the GCFR core support system, the rigid grid plate and single core element model will be replaced by a model using an elastic plate with multiple core elements. The new method will lead to natural frequencies that are lower than the frequencies calculated with the simplified model. However, it is expected that the new method of analysis will show increased damping and will produce lower amplitudes and stresses in the core components. The reason for this optimism comes from the fact that with a more realistic model, the conservative assumptions made with a simple model can greatly be reduced.

References

[1] REISSNER, ERIC, "On Axi-symmetrical Vibrations of Circular Plates of Uniform Thickness, Including the Effects of Transverse Shear Deformation and Rotary Inertia," J. Acous. Soc. Am., 26, 2, pp. 252-253 (1954).

[2] MINDLIN, R. D., DERESIEWICS, H., "Thickness-Shear and Flexural Vibrations of a Circular Disk," J. Appl. Phys., 25, 10, pp. 1329-1332.

[3] GREEN, A. E., ZERNA, W., Theoretical Elasticity, Clarendon Press, Oxford (1954).

[4] SZILARD, R., Theory and Analysis of Plates, Prentice-Hall, Inc. (1974).

[5] MCLACHLAN, N. W., Theory of Vibrations, Dover Publications, Inc. (1951).

[6] HURTY, W. C., "Dynamic Analysis of Structural Systems Using Components Modes," AIAA J., 3, 4, pp. 678-685 (April 1965).

[7] GLADWELL, G. M., "Branch Mode Analysis of Vibrating Systems," J. Sound and Vibration, I, pp. 41-59 (1964).

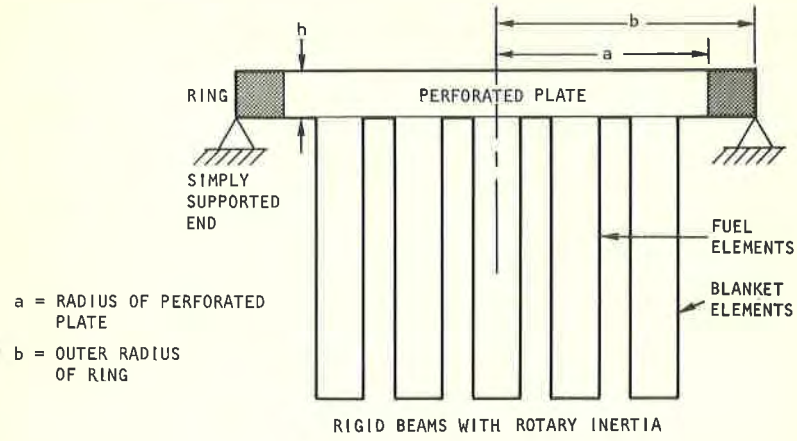

Fig. 1 Perforated plate with solid ring

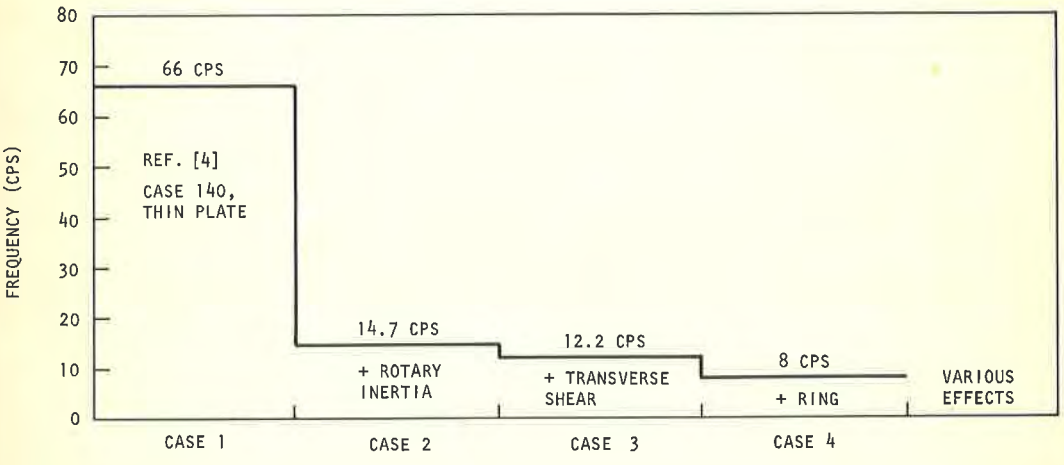

Fig. 2 Various effects on the Frequency of the grid plate

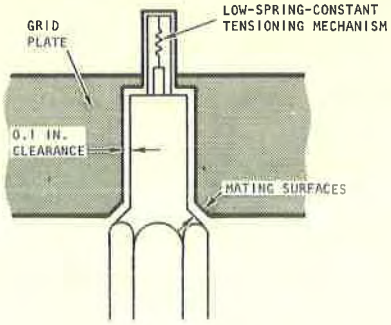

Fig. 3 Support of core element

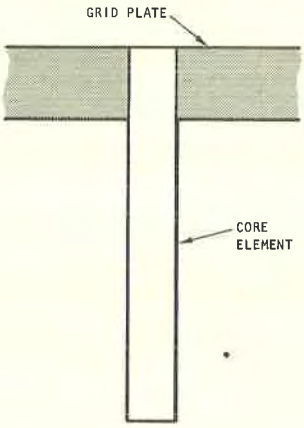

Fig. 4 Fixed end

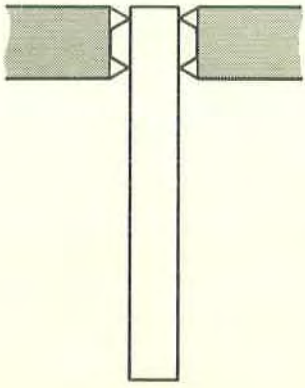

Fig. 5 Double hinges